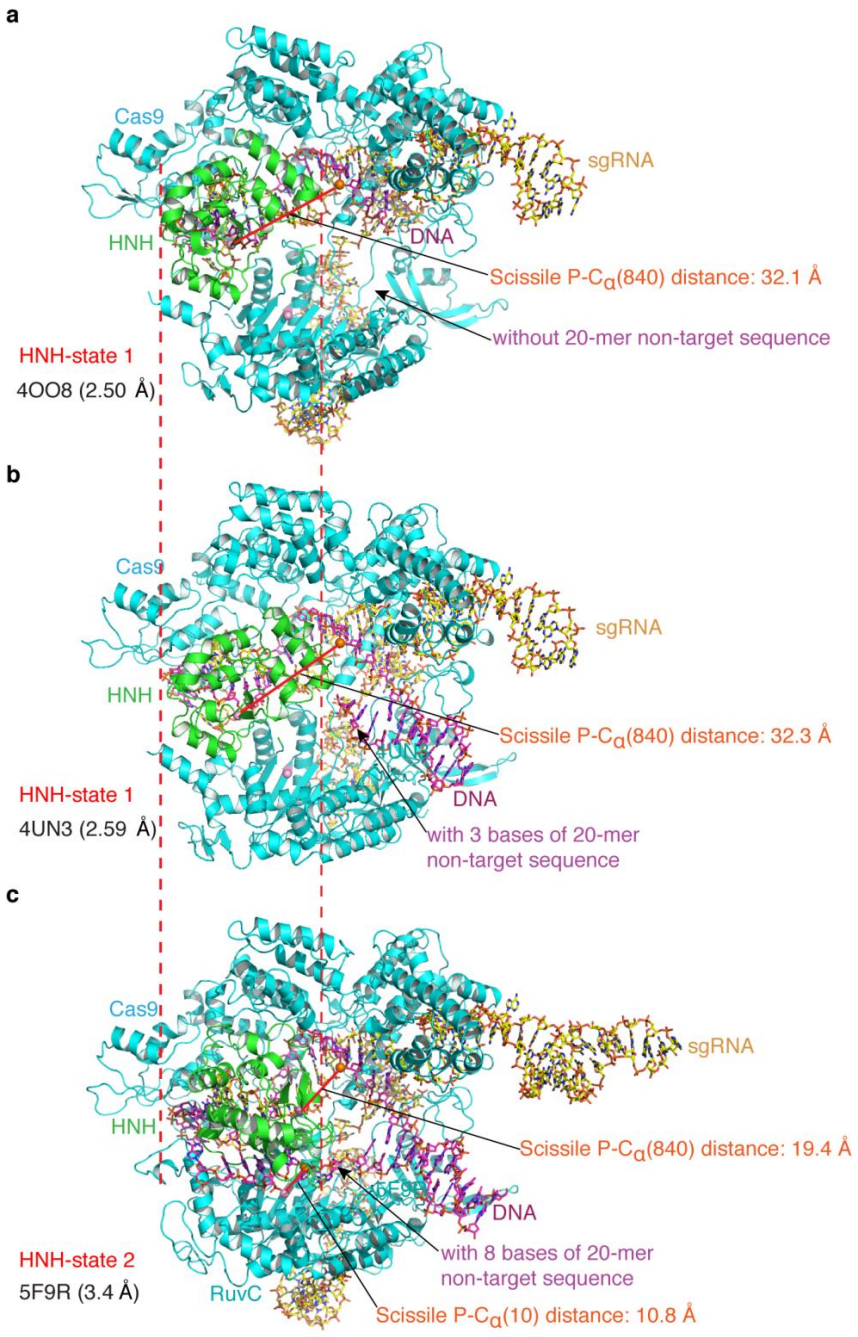

Supplementary Figure 1 | Two distinct conformational states of the HNH domain in crystal structures. a HNH-state 1 in PDB 4OO8, in which the distance from the C_α atom of the HNH catalytic residue 840 to the attacked phosphorus (scissile P) of the target strand is 32.1 Å. The dashed lines indicate the boundary of the HNH domain. **b** HNH-state 1 in PDB 4UN3, in which the distance from HNH-C_α(840) to its scissile P is 32.3 Å. **c** HNH-state 2 in PDB 5F9R, in which the distance from HNH-C_α(840) to its scissile P is 19.4 Å, and that from RuvC-C_α(10) to its scissile P of the non-target strand is 10.8 Å.

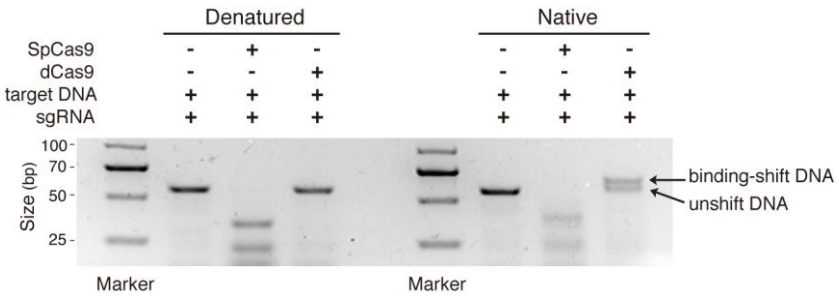

Supplementary Figure 2 | Detection of the formation of the SpCas9-sgRNA-DNA ternary complex by agarose gel electrophoresis. To ensure the ternary complex formation, a concentration ratio of 1:1.2:1.5 was used for SpCas9/dCas9(D10A, H840A), sgRNA and target DNA in the mixture. The electrophoresis was carried out after the mixture was cultured and dispersed overnight. Denatured: the mixture solution was heated at 70 °C for 10 min before electrophoresis to inactivate and disassociate the complexes. Native: electrophoresis without denaturation. In the last lane, the 'binding-shift' band indicates the target DNAs bound to SpCas9-sgRNA; and the 'unshift' band corresponds the remaining DNAs. Data are shown for one representative experiment from three independent experiments with similar results.

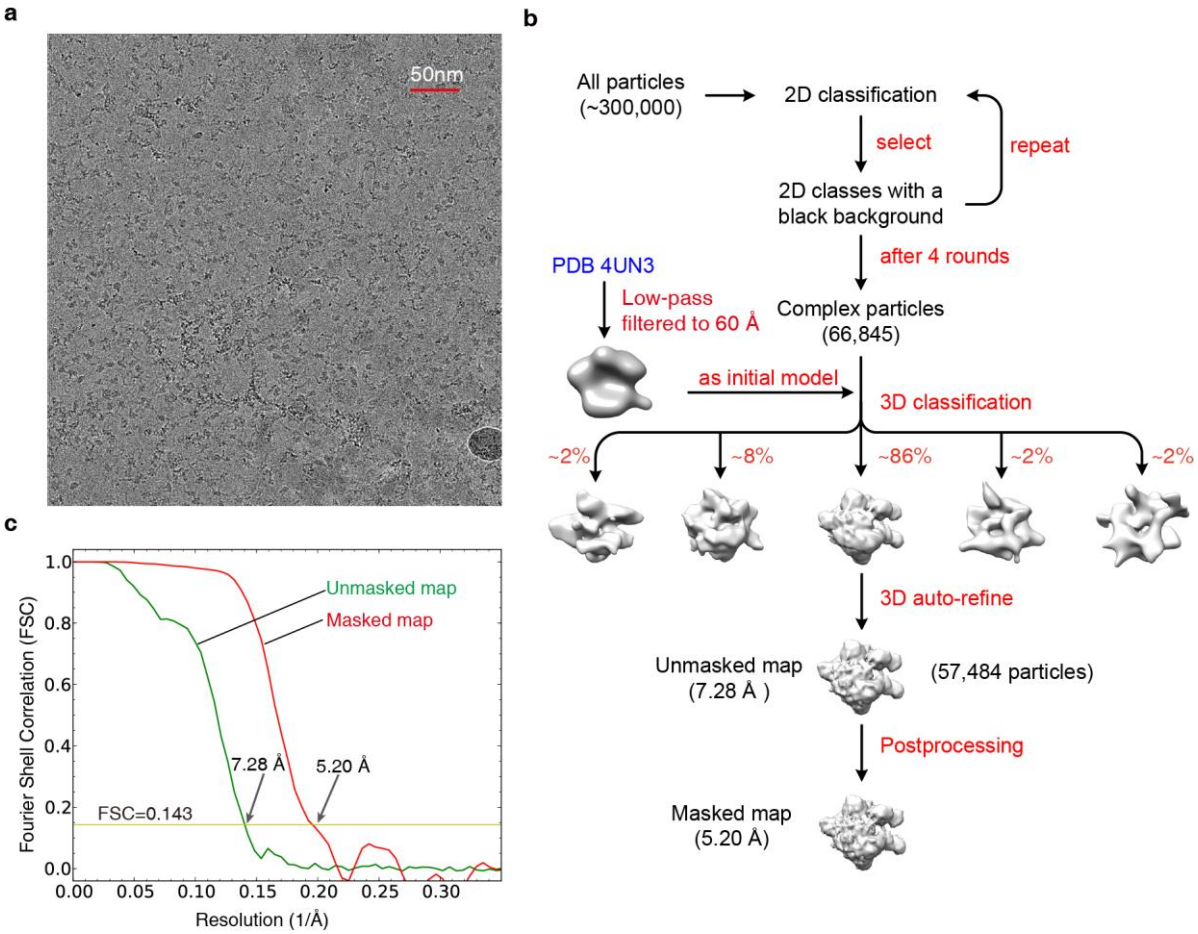

Supplementary Figure 3 | Single-particle cryo-EM study of the SpCas9-sgRNA-DNA ternary complex. a A typical raw micrograph of the ternary complex in the vitreous ice (scale bar, 50 nm). All cryo-EM images were collected on a Titan microscope using a K2 Summit direct detection device camera. **b** Flowchart for the single-particle 3D reconstruction with RELION. **c** FSC curves for the EM density maps between two independently refined halves, before and after post-processing in RELION.

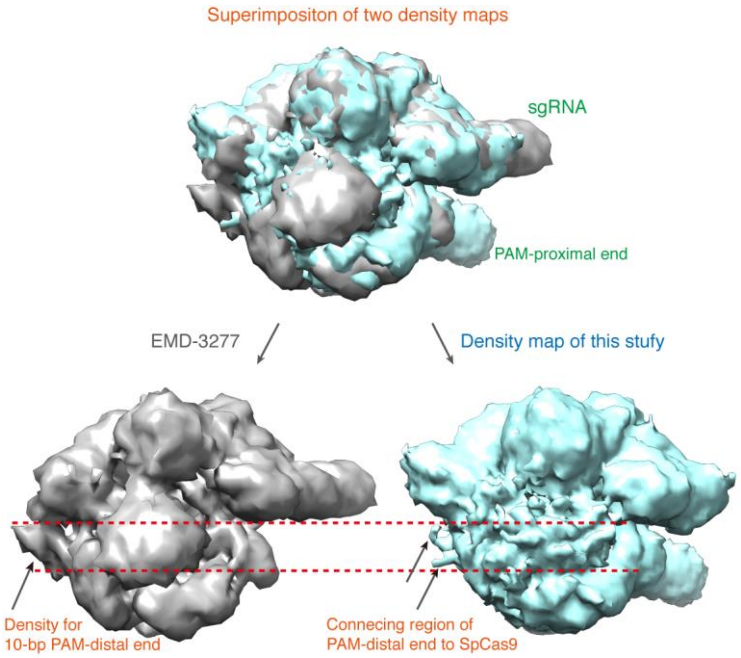

Supplementary Figure 4 | Superimposition of cryo-EM density maps of the ternary complex. The superimposition of our EM density map on (contoured at ~1.0σ) a recent EM structure with a 40-bp target DNA (EMD-3277, contoured at ~1.7σ) reveals relatively small density regions that may correspond to the connecting region of the PAM-distal end to SpCas9.

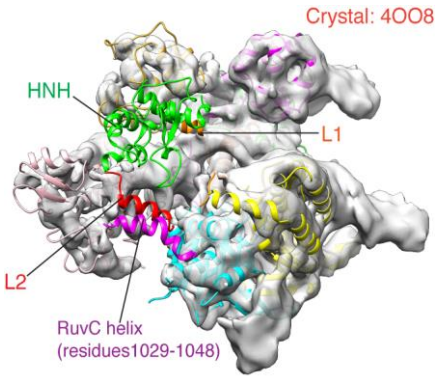

Supplementary Figure 5 | Rigid-body fitting of the crystal structure 4OO8 with the HNH domain. The correlation coefficient of the rigid-body fitting is ~0.80. The density map is shown at the contour level of ~4.0σ. Except for the helices in HNH, L1 and L2, and one in RuvC (residues 1029-1048), other helices in 4OO8 could be well resolved, as shown in Fig. 1c.

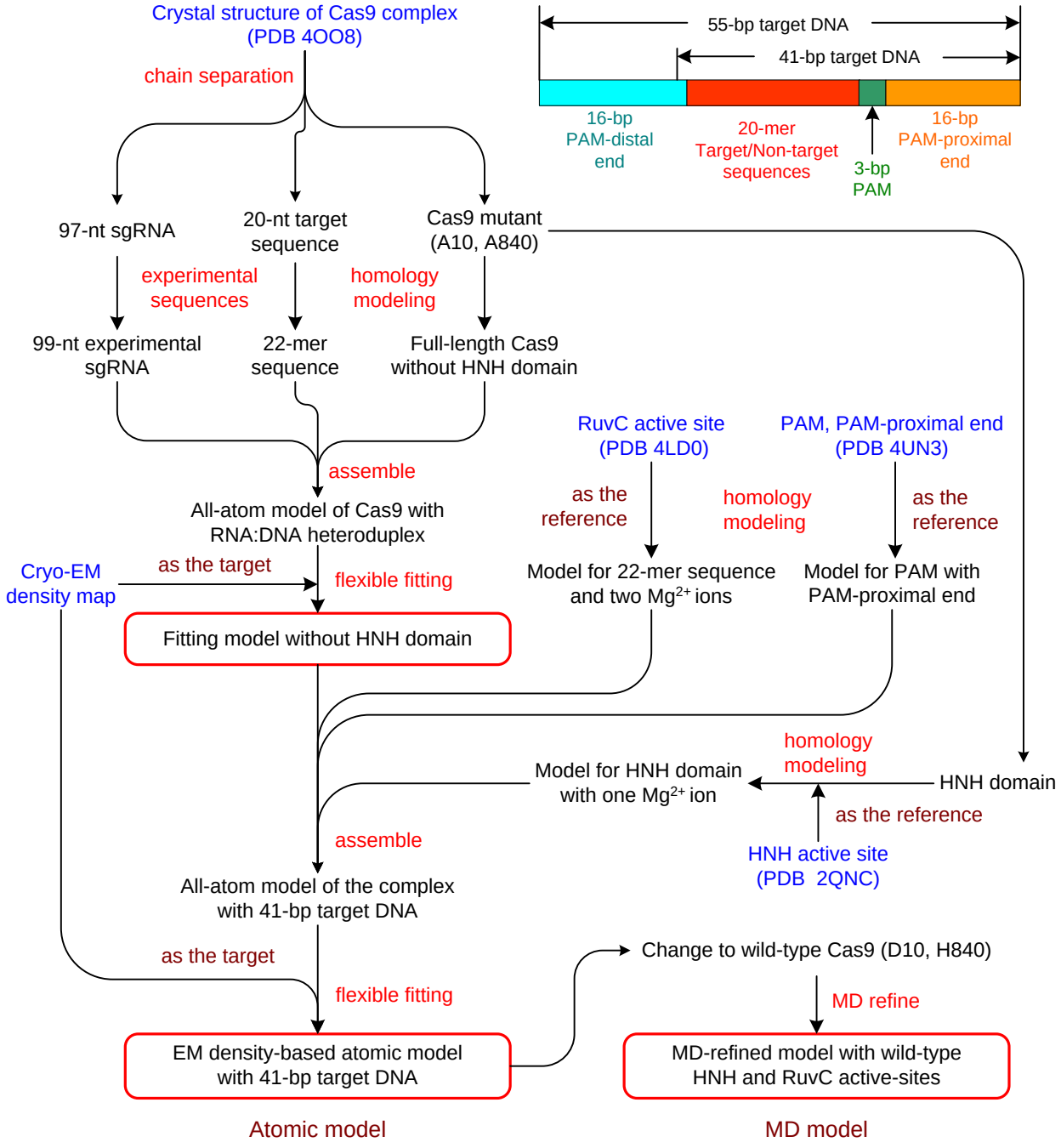

Supplementary Figure 6 | Flowchart for the building and refinement of atomic models. The atomic model for the ternary complex possesses the experimental SpCas9 mutant (D10A, H840A) and 41 base pairs of the 55-bp target DNA (41-bp target DNA). The MD model for the ternary complex with the wild-type SpCas9 was constructed with the EM-based atomic model, and then refined by large-scale MD simulations with explicit water solvent.

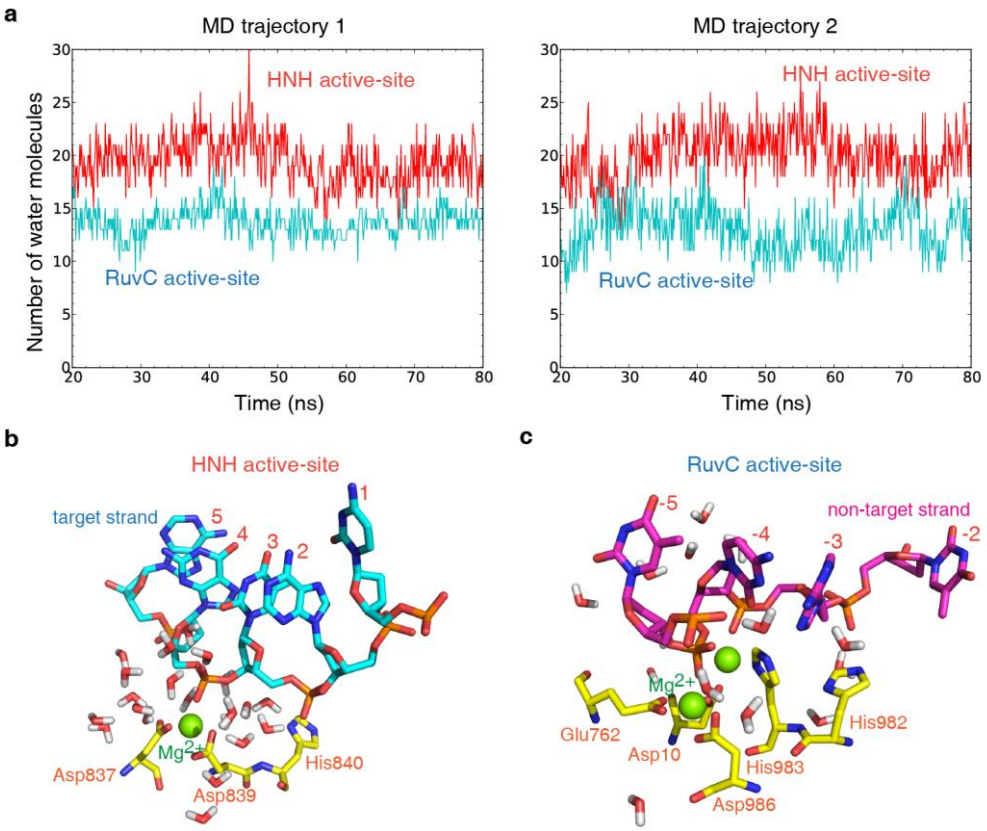

Supplementary Figure 7 | MD simulations of the ternary complex with explicit solvent. **a** Time-dependent number of water molecules in the wild-type HNH and RuvC active-sites in two independent MD simulations of 80 nanoseconds (ns). **b, c** Snapshots of water molecules in the HNH active-site (21 molecules within 7 Å around Mg^{2+}) and the RuvC active-site (14 molecules within 10 Å around two Mg^{2+} ions) at 50 ns from MD trajectory 2.

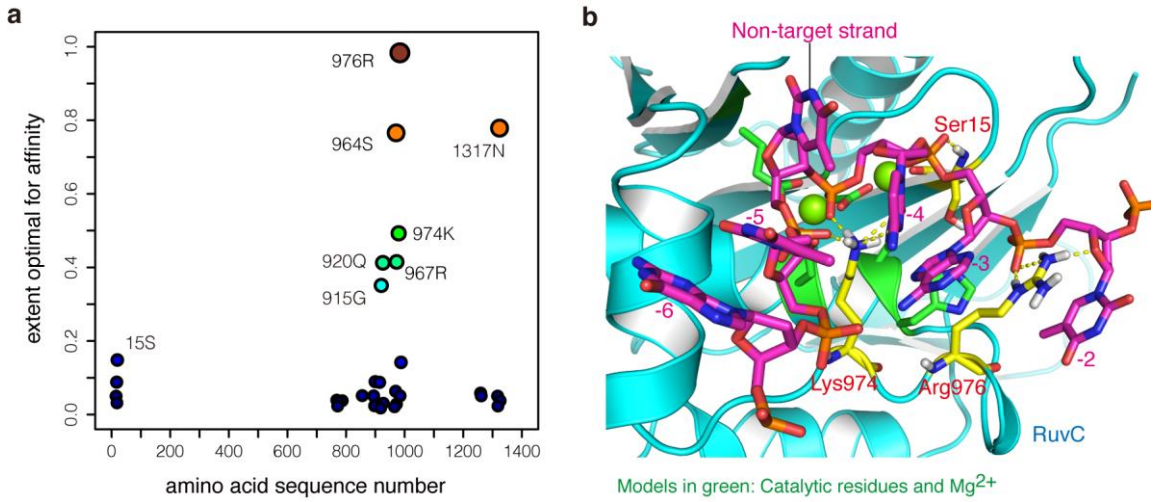

Supplementary Figure 8 | Key RuvC residues for the binding to the non-target strand. a Structure-based prediction of key residues using the MD-refined atomic model and the Rosetta program. The radius of each circle is proportional to the computational affinity score of the corresponding residue to the non-target DNA strand. **b** Hydrogen bonding of three key RuvC residues (in yellow) with the non-target strand in the MD model.

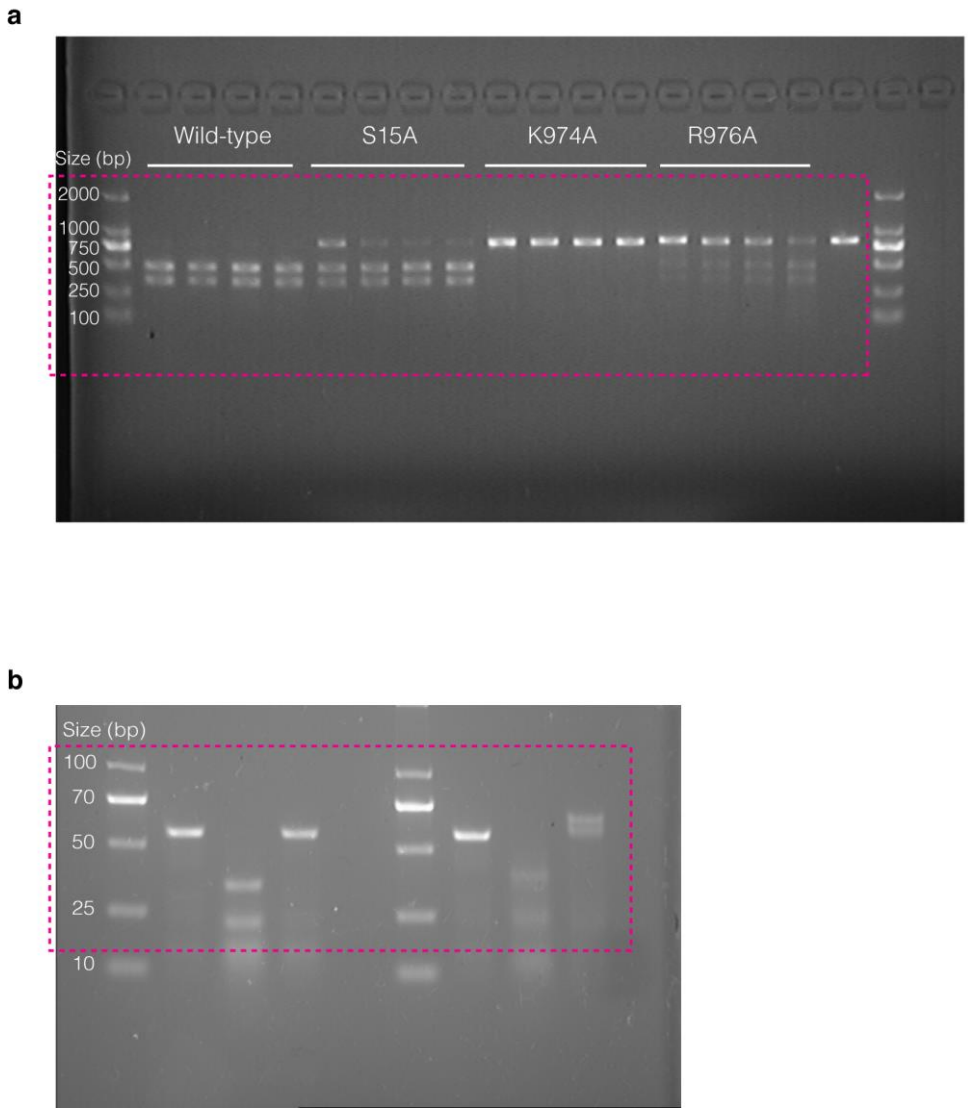

Supplementary Figure 9 | The uncropped images of agarose gel electrophoresis. a The uncropped image corresponding to Fig. 5c. The magenta box shows the region presented in the figure. **b** The uncropped image corresponding to Supplementary Fig. 2. The magenta box shows the region presented in the figure.

Supplementary Table 1 | Parameters of cryo-EM data collection and 3D reconstruction

Data collection	
Micrographs	592
Voltage (kV)	300
Pixel size (Å)	1.3
Total electron dose (e^{-} $Å^{-2}$)	45
Exposure time (s)	7.6
Nominal magnification	18000×
Defocus range (μm)	-1.3 to -3.5
3D reconstruction	
Final particles	57484
Resolution (Å)	5.20
Accuracy of rotation (degree)	5.12
Accuracy of translation (pixel)	1.83
B-factor ($Å^2$)	-80.0

Supplementary Table 2 | Primer sequences used in this study

Primer names	Sequences (5'→3')
Amplification of SpCas9 coding sequence	
Cas9-Half1F	CGCGCGGCAGCCATATGGAAAATCTCTACTTCCAAGGCG
Cas9-Half1R	CAGTTTTCTTGACAGCCGCC
Cas9-Half2F	GGCGGCTGTCAAGAAAACTG
Cas9-Half2R	TGGTGGTGGTGCTCGAGTCAGTCTCCACCGAGC
Construction of the dCas9 mutant(D10A, H840A)	
dCas-upF	GGAATTGTGAGCGGATAACAATTCC
dCas-10F	ATTGGGCTCGCTATCGGCACAAACAGCG
dCas-10R	CGCTGTTTGTGCCGATAGCGAGCCCAAT
dCas-840F	GACTACGACGTGGATGCTATCGTGCCCCAGT
dCas-840R	ACTGGGGCACGATAGCATCCACGTCGTAGTC
Construction of other SpCas9 mutants	
cas9 mut upF	GCGAAATTAATACGACTCACTATAGG
cas9 mut upR	CCGGGATTTGGACAGCC
15R	GCCGACGGCGTTTGTGCCGATATCG
15F	ACAAACGCCGTCGGCTGGGCCGT
cas9 mut downF	GGCGGCTGTCAAGAAAACTG
cas9 mut downR	TTAGCGTCGGCGAGGATC
974F	TTTATGCGGTGAGAGAGATCAACAATTACC
974R	CTCTCTCACCGCATAAAACTGAAAGTCCT
976F	TAAGGTGGCAGAGATCAACAATTACCACC
976R	GATCTCTGCCACCTTATAAAACTGAAAGTCC
sgRNA in vitro transcription	
gRNA-F	TAATACGACTCACTATAGGTACCGCTCCAGTCGTTCATGGTTTTAGAGCT
	AGAAATAGCAAGTTAAAAT
gRNA-R	AGCACCGACTCGGTGCCACT
DNA cleavage	
Invitro Cut F (Fam)	CTGTGAAGTCAACTTGTCAATCC
Invitro Cut R (Rox)	CCCTCCATGTACAGCTCTTCAT